Seismic Performance of X-Braces of Steel Equal-leg Angle

T. Yamashita
Kogakuin University, Tokyo, Japan

SUMMARY:
This paper describes an experimental study on the inelastic behavior of X-bracing of steel angles subjected to monotonic and cyclic loading, and specifies basic seismic performances, such as rigidity, ductility and energy dissipation. The diagonal bracing is set into 3.7m-square frame, and connected to the frame using high-strength bolt and gusset plates. The section of braces is equal leg angles of which the width -thicknesses are 60-5mm and 75-6mm. Moreover, the brace sections are of single angle and of composite section of two angles on both sides of the gusset plate are tested. It is found that the ductility of single angle brace is quite good despite the eccentricity and slenderness, and considerable hysteretic damping is found.

Keywords: X-brace, Equal leg angles, buckling, inelastic deformation, equivalent viscous damping ratio

1. INTRODUCTION

In Japan, X-braces are employed as anti-earthquake elements in many steel buildings, such as factories, school gymnasiums or station facilities, etc. Especially steel equal leg angles are popularly used as the section of such X-braces. But failure or severe buckling of such steel angle braces during great earthquakes are often reported (Hasegawa 2005, Murayama 2005).

In design of such slender X-braces, the strength of compressed brace is often neglected. However, the deformation capacity is strongly affected by buckling. Bending-torsional buckling occurs and many researches discuss about the buckling strength (Liu 2008, Arai 2000). However, when used as braces, performance for cyclic load is important. As for other sections, Kato et al (the AIJ annual 1990) conducted experiments of X braces of H-shaped steel for cyclic load and investigated inelastic deformation capacity. Yoo et al (Engineering Structures 2009) conducted detailed FE analysis of X-brace of rectangular hollow section to investigate the effects of joint detail on seismic performances. But real-scale experiments of X-braces of steel angle for cyclic load are few, as far as the author knows, in spite that angle-braces are popularly used in Japan.

In the present study, through real-scale tests of X-braces of steel angle for both monotonic and cyclic loads, basic anti-seismic performances, such as deformation capacity or energy dissipation, are investigated. The X-braces are diagonally installed into 3.7m square frame. The maximum story drift is approx. 0.04 rad.

2. EXPERIMENTS OVERVIEW

2.1. Setup of experiments

Fig.2.1 illustrates the setup. A 3.7m x 3.7m square frame was constructed using H-shaped steel and the X-braces were installed to the diagonals. The material of H-shaped steel was SS400 (JIS 2004) and the H-350x175x7x11 section was used to avoid yield or bucking preceding the yield of diagonal braces.

To minimize the horizontal stiffness of frame itself, a web-connection illustrated in Fig.2.2, was employed to connect the column and beam in the frame. The frame was fixed at the bottom to the thick concrete floor slab of the facility using PC-bars. The load was given at the left of top beam using an oil-jack.

The sections of diagonal X-brace were single and double angles. For the single-angle brace, the L-60x5 and L-75x6 sections were used. The notation "L-60x5" represents single angle section in which the nominal equal leg length is 60mm and the thickness is 5mm, for example. For the double angle sections, the 2L-65x6 and 2L-75x6 sections were used. The two angles were connected to each other at interval of 550mm by high strength bolts and inserted plates between two angles. The SS400 steel was also used for these braces. The mechanical properties are given in Table.2.1. The thicknesses of used angle sections were slightly less than the nominal. Therefore, the section properties to analyse the experimental data, are calculated from the nominal values assuming proportion to the thickness (see also Table 2.1).

All the braces were connected to gusset plates. The thicknesses of gusset plate were 9mm for L-60x5, L-75x6 and 2L-60x5 and 12mm for 2L-75x6. Five high strength bolts were used per one joint. The connection detail was designed in accordance with the Building Standard Law of Japan (BSL 2007) which demanded yield over the full-length of brace preceding the joint failure.

2.2. Load and monitoring

In the experiments, two load patterns, monotonic and cyclic, were given to each section. However, monotonic load test using the 2L-60x5 brace could not be conducted because of a construction trouble.

The given load was measured using a load-cell set at the jack head (Fig.2.1). The horizontal displacements at the two column heads were also measured by two displacement gages (Fig.2.1). The average of two measured horizontal displacements at each column head (denoted by δ) was taken to express the deformation of brace. Forced displacement was manually given monitoring the value of δ. The maximum limit of displacement was 140mm due to the capacity of gages. The loading velocity

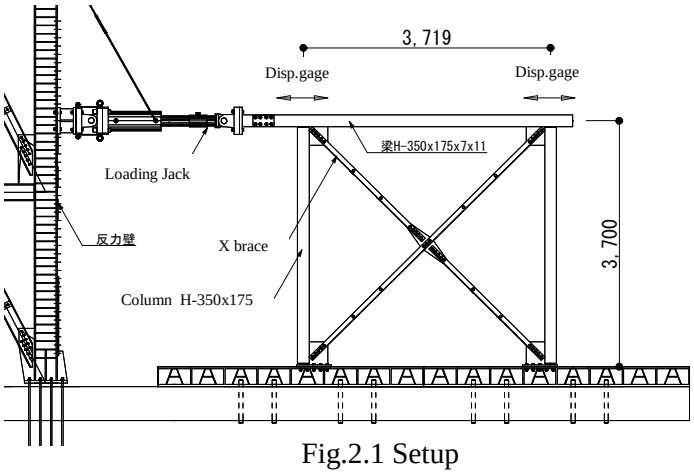

Fig.2.1 Setup

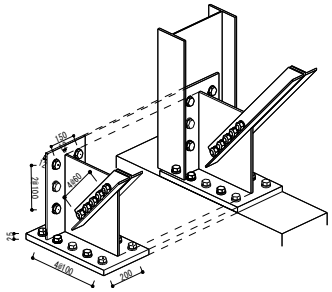

Fig.2.2 Joint Detail

Table 2.1 Data of Braces

	Unit	L-60x5	L-75x6	2L-60x5	2L-75x6	L-60x5	L-75x6	2L-60x5	2L-75x6
Load		Monotonic				Cyclic			
Yield strength	N/mm^2	345	305		305	345	305	345	305
Tensile strength	N/mm^2	460	424		424	460	424	460	424
Equal leg length(Nominal)	mm	60	75		75	60	75	60	75
Thickness(Nominal)	mm	5.0	6.0		6.0	5.0	6.0	5.0	6.0
Section area(Nominal)	cm^2	5.802	8.727		17.454	5.802	8.727	11.604	17.454
Thickness(Measured)	mm	4.6	5.7		5.7/5.7	4.5	5.6	4.6/4.6	5.6/5.7
Gusste thickness	mm	9	9		12	9	9	12	12
High Strength Bolt		5-M16	5-M20		5-M20	5-M16	5-M20	5-M16	5-M20

was very low.

The amplitude in the cyclic load was gradually increased. Table 2.2 indicates the amplitudes for each cycle. When the amplitude was less than or equal to 40mm, two cycles were given at one amplitude. The story drift angle γ is defined by Eq.(2.1) in terms of δ (see Fig.2.2)

$$\gamma = \frac{\delta}{l_o \sin\theta} \tag{2.1}$$

The axial strain of brace is estimated as follows. Assuming that the gusset is rigid, and ignoring the bending strain due to eccentric joint, the compatibility equation between the horizontal displacement δ and axial strain of brace ε_t is expressed by Eq.(2.2) considering the axial deformation of column and beam(see Fig.2.3).

$$\delta = l_e \cdot \left(\frac{1}{\cos\theta}\varepsilon_t + \frac{\sin^2\theta}{\cos\theta}\varepsilon_c + \frac{\cos\theta}{2}\varepsilon_b \right) \tag{2.2}$$

where ε_c and ε_b are the axial strain of column and beam of the square frame, respectively. The equilibrium between the axial forces leads to Eq.(2.3).

$$\varepsilon_c = \frac{N_t \sin\theta}{EA_c}, \quad \varepsilon_b = \frac{N_t \cos\theta}{EA_b} \tag{2.3}$$

where A_c and A_b are the section areas of column and beam, respectively, N_t is the axial force of brace. Elato-plastic bilinear relation between N_t and ε_t is assumed.

$$\begin{aligned} N_t &= EA\varepsilon_t \quad (\varepsilon_t \le \varepsilon_y) \\ N_t &= EA\varepsilon_y \quad (\varepsilon_t > \varepsilon_y) \end{aligned} \tag{2.4}$$

Substituting Eqs.(2.3) and (2.4) into Eq.(2.2), an expression of ε_t in terms of δ is derived.

$$\varepsilon_t = \begin{cases} \dfrac{\delta}{\left(\dfrac{1}{\cos\theta} + \dfrac{\sin^3\theta}{\cos\theta}\dfrac{A}{A_c} + \dfrac{\cos^2\theta}{2}\dfrac{A}{A_b} \right) l_e} & (\varepsilon_t \le \varepsilon_y) \\ \left\{ \dfrac{\delta}{l_e} - \left(\dfrac{\sin^3\theta}{\cos\theta}\dfrac{1}{A_c} + \dfrac{\cos^2\theta}{2}\dfrac{1}{A_b} \right) A\varepsilon_y \right\} \cos\theta & (\varepsilon_t > \varepsilon_y) \end{cases} \tag{2.5}$$

Fig.2.4 indicates the correlation between the axial strain calculated by Eq.(2.5) and the story drift angle for the L-60x5 and 2L-75x6 braces. They almost coincide and the correlations are almost linear. In the calculation of above Eqs (2.1)-(2.4), 45 degrees and 4240mm are given as the value of θ and l_e.

Table 2.2 Amplitudes in cyclic load

Amplitude δ (unit:mm)	Story drift angle γ (unit:rad)	Cycles
5	0.001	2
10	0.003	2
15	0.004	2
20	0.005	2
25	0.007	2
30	0.008	2
35	0.009	2
40	0.011	2
50	0.014	1
60	0.016	1
70	0.019	1
80	0.022	1
100	0.027	1
120	0.032	1
140	0.038	1

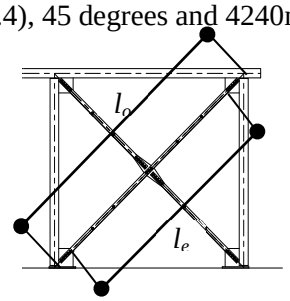

Fig.2.2 Brace length

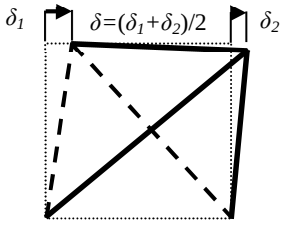

Fig.2.3 Deformation of braced frame

Fig.2.4 Axial strain of brace

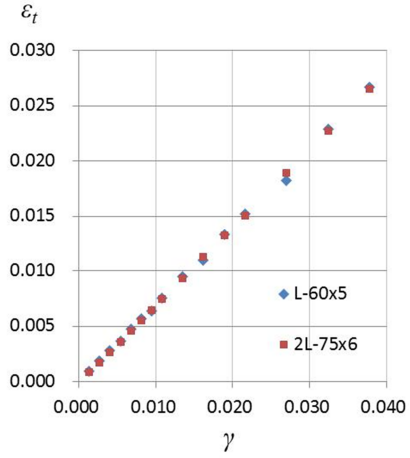

3. INELASTIC BEHAVIOR

3.1. Monotonic loading tests

3.1.1. Behavior of tensioned brace

When subjected to the monotonic load, stable inelastic behaviour of the tensioned brace was observed. No failure of brace and slip of bolts were found until the limit story drift of 0.04 rad.

As shown in Fig.3.1, the axial strain at the midpoint of brace remained low until the story drift of 0.01 rad but began to rapidly increase after that. It leads a presumption that the overall axial strain of tensioned brace causes at the story drift of 0.01rad. At 0.02rad, the mill scale began to come off all over the brace.

3.1.2. Behaviour of buckled brace

Buckling caused at the compressed brace. But it did not cause at the both two compressed braces but only one brace was buckled. Table3-1 shows the location of buckling. As for the single-angle braces, slight buckling was observed at the story drift of 0.0016 rad., and it became clearly identifiable at the drift angle of 0.005 rad. (Fig.3-3). Bending-torsional buckling was observed. Moreover, (as also reported by Hozumi et al ()), the angle section at the break point of buckling significantly flattened (Fig.3.4) and the brace bent very smoothly. This flattening of section prevented local buckling.

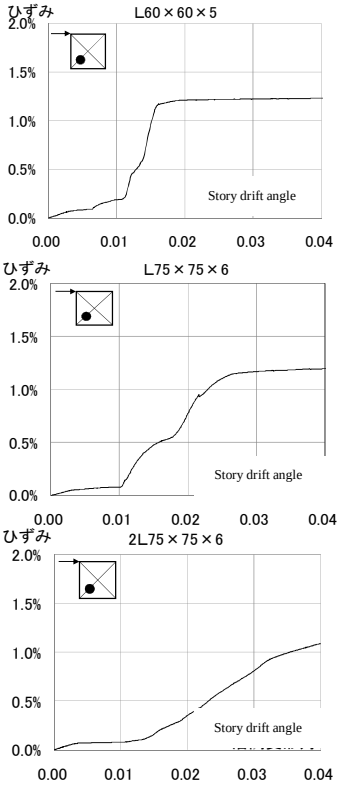

Figs.3.1 Axial strain at midpoint of brace

Table.3.1 Location of buckling or failure

	L-60x5	L-75x6	2L-60x5	2L-75x6
Monotonic load				
Cyclic load				

▼ : Failure
▽ : Buckling accompanying local buckling
○ : Buckling without local buckling

Figs.3.3 Buckling at the story drift of 0.005 rad.

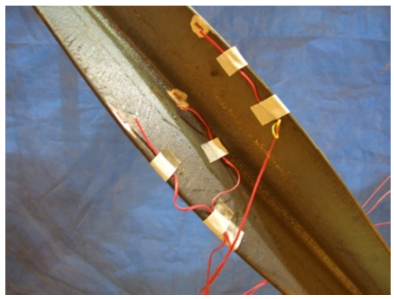

Fig.3.4 Flattening of section at break point

On the other hand, severe local buckling was observed at the break point of the double angle braces (Fig.3.5). Bending-torsional buckling accompanying the flattening of section such observed in the case of single-angle brace did not occur. This local buckling leads to very large bending strain and low-cycle fatigue failure for cyclic load.

Fig.3.5 Break point of 2L-75x6 brace

3.2. Cyclic loading tests

3.2.1. Behaviour of single-angle brace

Table3-1 also shows the location of buckling and failure when subjected to the cyclic load. As shown above, local buckling did not occur at the break point of single-angle brace. Thus low-cycle fatigue failure at the break point did not occur as for the L-60x5 brace. But the failure at the first bolt at the lower gusset connection caused at the story drift of 0.03rad (Fig.3.6). As for the L-75x6 brace, failure and slip of the bolts did not occur until the maximum story drift of 0.04 rad.

3.2.2. Behaviour of double-angle brace

In contrast to the mild behaviour of single-angle braces, the double-angle braces buckled accompanying severe local buckling at the break point. At first, in-plane buckling was observed where the break point of braces was just at the midpoint without intermediate connection bolt. But the buckling mode gradually transformed to out-of-plane buckling accompanying the growth of local buckling especially at the inner angle. The final buckling modeshape and location of the break point of the 2L-75x6 brace differed from those for the monotonic load. Finally, failure occurred at the drift angle at around 0.01 rad. for both the 2L-60x5 and 2L-75x6 braces. The location of failure was the break point at the midst for the 2L-60x5 brace (Fig.3.7). But as for the 2L-75x6 braces, the failure location was not at the break point but at the local buckling at the intermediate connection bolt, that caused after the general buckling (Fig.3.8).

4. RESTORING FORCE CHARACTERISTICS

4.1. Load-displacement curve

The yield strength of brace for non-dimensioning the experimental inelastic strength is determined by Eq.(4.1).

$$Q_{yo} = \sigma_y A \cos\theta \tag{4.1}$$

in which σ_y and A is the actual yield strength and section area of brace, respectively. Figs.4.1 shows the non-dimensioned load-displacement curves for the monotonic load and Figs.4.2 shows those for the cyclic load. The X-axis is the story drift angle γ.

Fig.3.6 Failure of L-60x5

Fig.3.7 Failure of 2L-60x5

Fig.3.8 Failure of 2L-75x6

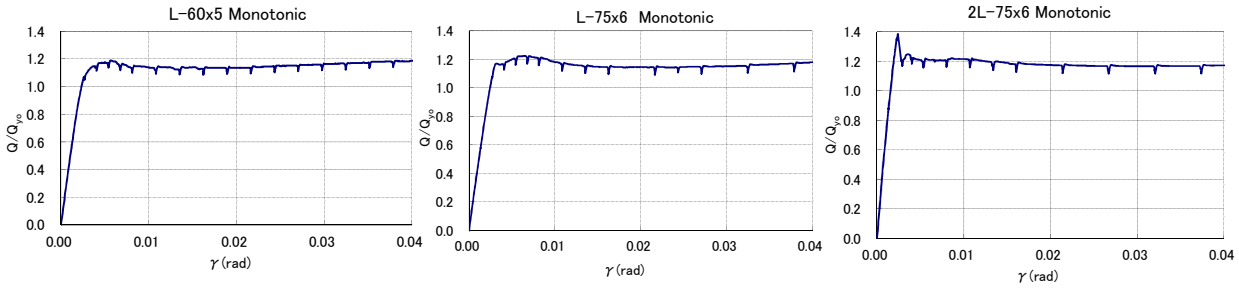

Figs.4.1 Load-displacement curves for monotonic load

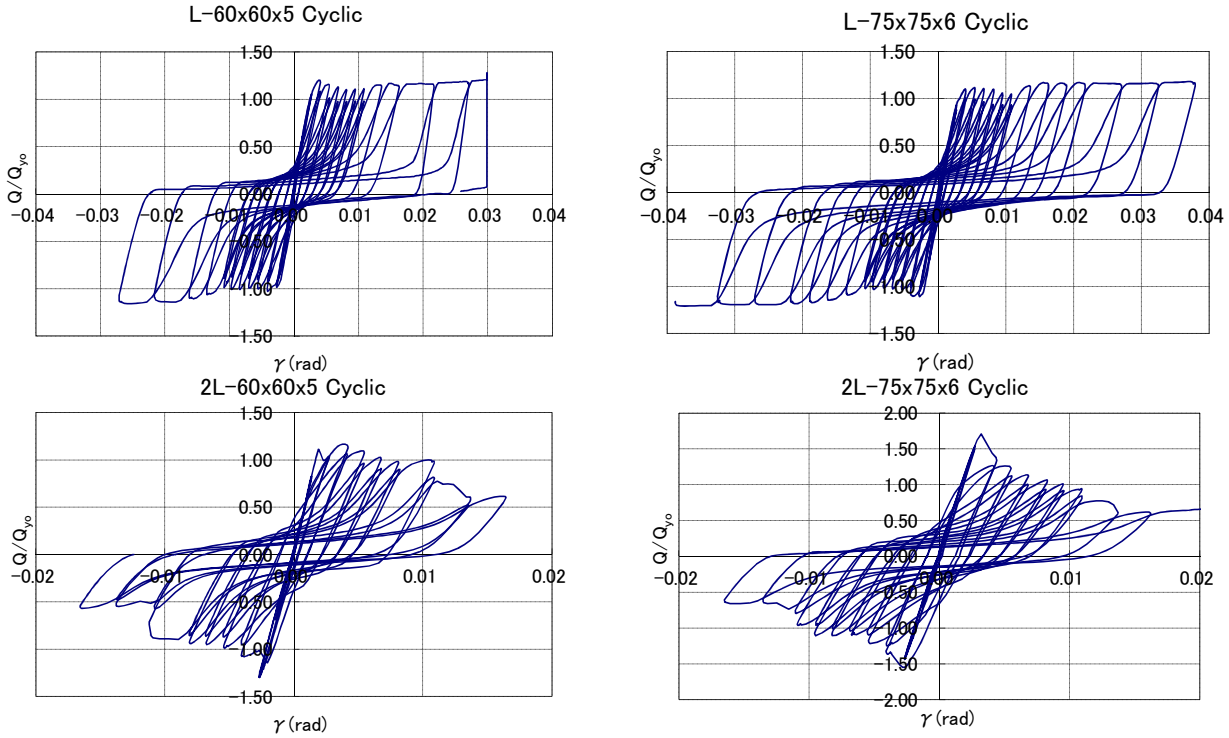

Figs.4.2 Load-displacement curves for cyclic load

The load is the sum of the brace and frame strengths. But the exact separation of measured load at the jack-head into these two components is difficult. Fig.4.3 shows the load-displacement curve of the square frame without diagonal braces. This frame experiment was conducted after the completion of all the brace experiments. The frame strength was low. At the drift angle of 0.04 rad., it was 23kN, only 18% of the minimum of Q_{yo} (of the L-60x5 brace). Although the inclinations for the positive and negative displacement are different, the load-displacement relations seem to be almost linear.

To extract the strength of braces, the frame strength Q_f is approximated as two linear functions (for plus and minus sides) of the story drift angle γ.

$$Q_f = \begin{cases} 575\gamma & (\gamma \geq 0) \\ 300\gamma & (\gamma < 0) \end{cases} \quad \text{(unit: kN)} \qquad (4.2)$$

The function of Eq.(4.2) is shown in Fig.4.3 by the bold lines.

Assuming that Q_f is commonly applicable for all the tests, the strength of brace itself is extracted by deducing Q_f from the measured load at the jack-head.

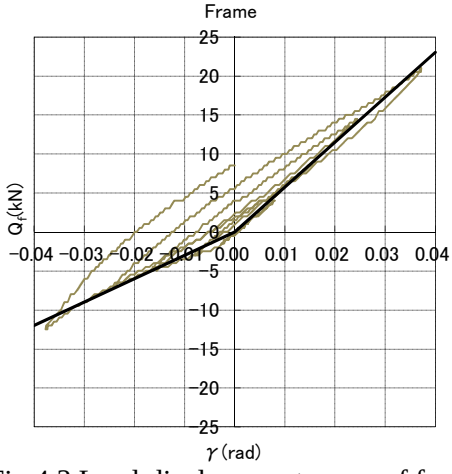

Fig.4.3 Load-displacement curve of frame

4.2. Slenderness and compressive strength

In structural design of ordinary X-braces, only tensioned brace is assumed to be effective and compression brace is often neglected when the braces are slender. However, buckling is strongly related to the deformation capacity and energy absorption. Thus an evaluation of slenderness and compressive strength is required.

The slenderness is given by Eq.(4.3).

$$\lambda_c = \sqrt{\frac{N_y}{N_e}}, \quad \left(N_y = \sigma_y A \quad , N_e = \frac{\pi^2 EI}{l_b{}^2} \right) \tag{4.3}$$

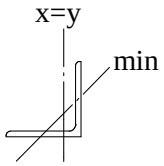

Fig.4.4 Axes of angle section

where E is the Young's modulus (=2.05x10^{5}N/mm^2), I is the second moment of inertia concerning buckling, l_b is the buckling length.

As stated in the previous section, bending-torsional buckling caused to the single-angle brace. However, how to evaluate the slenderness of such bending-torsional buckling is not established as far as the author knows. Therefore, a simple method given in the AIJ standard*) is employed herein. For the single-angle braces, $l_o/2$ (Fig.2.2) is determined to be the buckling length. The second moment of inertia about the "min." axis (Fig.4.4) is employed.

To determine the slenderness of double-angle braces, the maximum of the values for out-of-plane and in-plane buckling is taken. For out-of-plane buckling, the slenderness is calculated in accordance with a composite member regulation in the AIJ standard (AIJ 2004). For in-plane buckling, $0.4l_o$ is taken assuming that the gusset is rigid and the crossing joint is pin. In this case, the second moment of inertia about the "x=y" axis is employed.

The compressive strength of braces in the experiments (denoted by $N_c{}^{ex}$) is calculated by Eq.(4.4).

$$N_c{}^{ex} / N_y = \sqrt{2}\left(\frac{P_{\max} - Q_f}{Q_{yo}} - 1 \right) \tag{4.4}$$

in which P_{max} is the maximum measured load at the jack head. Q_f is calculated using Eq.(4.2) in accordance with the story drift angle at P_{max}.

On the other hand, the estimated compressive strength (denoted by $N_c{}^{es}$) is calculated by applying Eq.(4.5), that is given in the AIJ standard*).

$$N_c{}^{es} / N_y = \begin{cases} 1 - 0.24\lambda_c{}^2 & \left(\lambda_c \le 1/\sqrt{0.6} \right) \\ 1/\lambda_c{}^2 & \left(\lambda_c > 1/\sqrt{0.6} \right) \end{cases} \tag{4.5}$$

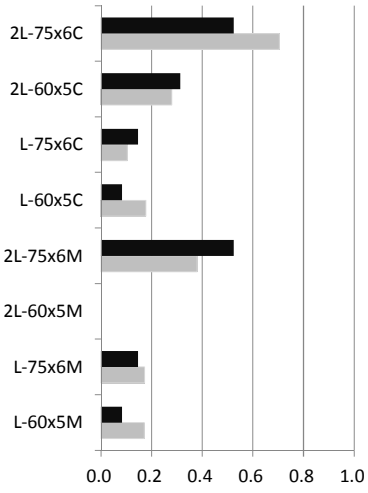

Fig.4.5 $N_c{}^{es}$ and $N_c{}^{ex}$

Table 4.1 Slenderness and compressive strength

Brace		L-60x5	L-75x6	2L-75x6	L-60x5	L-75x6	2L-60x5	2L-75x6
Load		Monotonic			Cyclic			
Bending-torsional buckling	l_b	$0.5l_o$	$0.5l_o$	$0.5l_o$	$0.5l_o$	$0.5l_o$	$0.5l_o$	$0.5l_o$
	λ_c	2.90	2.18	1.03	2.90	2.18	1.32	1.03
In-plane buckling	l_b			$0.4l_o$			$0.4l_o$	$0.4l_o$
	λ_c			1.12			1.49	1.12
$N_{cr}{}^{es}/N_y$		0.08	0.15	0.52	0.08	0.15	0.31	0.52
$N_{cr}{}^{ex}/N_y$		0.17	0.17	0.38	0.18	0.10	0.28	0.70

Table 4-1 contains the slenderness and compressive strength. Fig.4.5 compares N_c^{ex} and N_c^{es}. As a whole, they show considerably good agreement but the discrepancies are not small. For example, N_c^{ex} and N_c^{es} are close in the monotonic load test of the L-75x6 brace. But in the cyclic load test, N_c^{ex} is much less than N_c^{es}. As for the 2L-75x6 brace, N_c^{ex} is less than N_c^{es} in the monotonic load test, but it becomes reverse in the cyclic load test. These discrepancies might be due to initial stress or deflection caused by construction error. However, the slenderness in Table 4-1 is considered to be precise enough to survey the buckling behaviour. In addition, development of precise evaluation method for bending-torsional buckling strength of such gusset-connected angles is required.

4.3. Deformation capacity

4.3.1. Determination of elastic limit

Determination of elastic limit deformation is required to analyse the inelastic deformation capacity. The identification of elastic limit from the experimental load-displacement curves is difficult because of the effect of buckling of compressed brace or bending due to the joint eccentricity. Therefore, it is determined using Eq.(2.3). By substituting the yield strain ε_y into Eq.(2.3), the elastic limit displacement δ_{yo} and story drift angle γ_y are determined.

4.3.2. Inelastic deformation capacity

The inelastic deformation capacity is defined as the maximum deformation where the strength of brace holds Q_{yo}. In the monotonic load tests, the load-displacement curves are alike the elasto-plastic bilinear (Figs.4.1) and all the deformation capacities reach the story drift angle of 0.04 rad. On the other hand, for cyclic load, remarkable difference between the single- angle and double-angles are observed.

The single-angle braces show good deformation capacity. It reaches 0.027 rad. for the L-60x5 brace and 0.04 rad. for the L-75x6 brace. In contrast to that, the deformation capacities of the 2L-60x5 and 2L-75x6 braces are only 0.0068 rad. and 0.0094 rad., respectively. Local and overall buckling simultaneously occurred and had synergistic effect. This degrades not only compressive but also tensile strength because a deep fold due to local buckling is not fully stretched when subjected to tension again, or the effective area for tension decreases due to crack.

To evaluate the deformation capacity, the ductility factor μ is introduced.

$$\mu = \frac{\delta_{\max}}{\delta_{yo}} \tag{4.6}$$

where δ_{max} is the displacement corresponding to the deformation capacity. Also, the non-dimensioned strain energy η_n is defined by Eq.(4.7).

$$\eta_n = \frac{W_e + W_p}{Q_{yo}\delta_{yo}} \tag{4.7}$$

in which W_e and W_p are the elastic and plastic strain energies, respectively. The energy at the end of the hysteresis loop (when two cycles are given at a same amplitude, the energy at the end of the second cycle) corresponding to the deformation capacity is taken.

Table 4-2 contains μ and η_n of each brace. As for the double-angles braces for the cyclic load, the values of μ and η_n are very poor especially on the 2L-60x5 brace (μ=2.3 and η_n=11). In contrast, those of the single-angle braces are excellent, μ=9 and η_n=55 for the L-60x5 and μ=15 and η_n=94 for the L-75x6 brace.

Table 4.2 Inelastic deformation capacity

	unit	L-60x5	L-75x6	2L-75x6	L-60x5	L-75x6	2L-60x5	2L-75x6
Load		Monotonic			Cyclic			
Deformation	mm	140	140	140	100	140	25	35
capacity	rad	0.040	0.040	0.040	0.027	1/26	1/148	1/106
μ		13	15	14	9	15	2.3	3.4
η_n		15	16	16	55	94	11	32

4.4. Equivalent viscous damping

Damping due to energy dissipation is a very important performance of anti-earthquake elements. Equivalent viscous damping ratio h_{eq} is often employed as an index for the damping effect. h_{eq} is defined by Eq.(4.8)*).

$$h_{eq} = \frac{1}{4\pi} \cdot \frac{\Delta W}{W} \tag{4.8}$$

where ΔW is the area enclosed by a hysteresis loop corresponding to a load cycle. W is the elastic strain energy for the maximum deformation of the loop and corresponding strength.

Figs.4.9 show the correlation between the equivalent vicious damping ratio and the ductility factor for the amplitude of each cycle. For two cycles at same amplitude, two values for the first and second cycles are individually calculated. The continuous curve is given by a provision in the limit strength calculation in the BSL of Japan (BSL 2007). It is to calculate the inelastic response of bracing structures.

In spite of large slenderness, the equivalent viscous damping ratio holds more than 0.15 even at the single-angle braces. The value is retained from small deformation. At the double-angles braces, the damping ratios are much higher. Figs.4.10 show the extracted hysteresis loops at the story drifts of 0.004 and 0.008 rad. Both the first and second loops for 0.004 rad. where inelastic deformation is small, do not draw general slip-like shape but more swelled shape enclosing larger areas, thus the equivalent viscous damping becomes considerable. Observing the loops for 0.008 rad., the shapes of the single and double braces are almost same. In addition, the difference between the first and second loop shapes is small. Anyway, the dissipated energy is much larger than that of general slip model at such small deformation level.

The loops of single-angle brace for 0.014 rad. draws slip-like shape. As for the double-angles braces, significant degradation due to the local buckling, is observed.

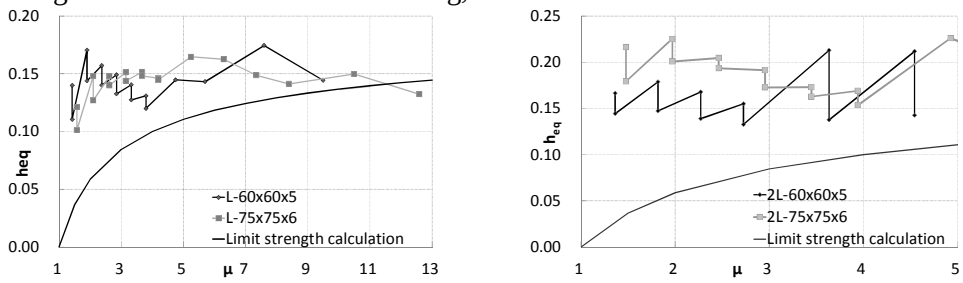

Figs. 4.9 Equivalent Viscous Damping

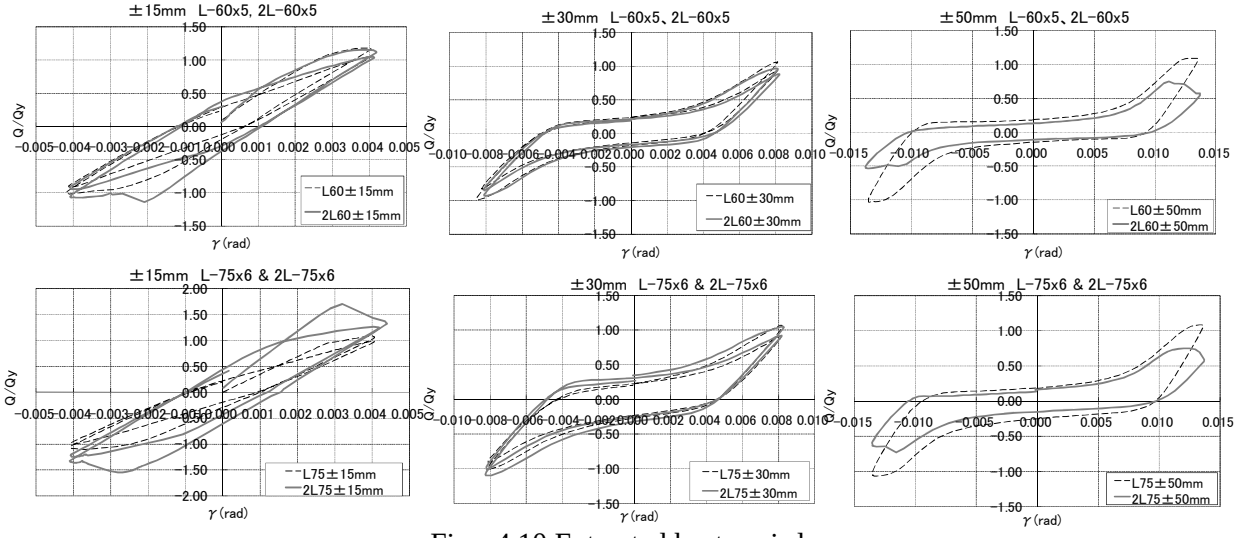

Figs. 4.10 Extracted hysteresis loops

5. CONCLUSIONS

Through the full-scale experiments of X-braces of steel angles, some important overviews about the seismic performance of such X-braces are obtained. They are summarized as follows;

1) The single-angle braces show excellent inelastic deformation capacity. This is due to the flattening of section at the break point, where concentration of strain is avoided.
2) In contrast to that, the deformation capacity of the double-angles is very poor because of severe local buckling at the break point.
3) The energy dissipation is considerable even on the slender single-angle braces. The equivalent viscous damping ratio holds near 0.15 from small deformation.

Based on the above findings, it is concluded that the seismic performance of steel X-braces of single-angle is excellent. However, when using double-angles braces such as those in the present experiments, the inelastic deformation capacity should be paid attention to.

AKCNOWLEDGEMENT

The author expresses his gratitude for the Urban Disaster Mitigation Center of Kogakuin University for supplying the finance for the present research. He is also grateful to Mr. Akihito Ozawa, Jun Yamazaki, Seiji Nagai and Yusuke Noguchi, who carried out the experiments together with the author.

REFERENCES

Hasegawa, T., Mukai, A., Nishida, K., and Ishihara, N.(2005). Damage investigation of steel gymnasiums due to the Niigataken-chuetsu Earthquake : Part 1 Study on structural damage. *The AIJ annual meeting (2005)*. B-2, 569-570 (in Japanese).

Murayama, F., Kozuka, A., and Doi, M.(2005). Study on Seismic Performance of existing steel gymnasiums in heavy snowfall area : Part 1 Condition of seismic damage in mid Niigata Pref. Earthquakes. *The AIJ annual meeting (2005)*. C-1, 597-598 (in Japanese).

Arai, S., Hongo, E., Ogawa, M., Yamazaki, T. and Fukasawa, T. (2000). Study on flexural torsional buckling of 690N/mm^2 high tensile steel angels for steel tower. *The AIJ annual meeting (2000)*. C-1, 453-454 (in Japanese).

Liu, Y. and Hui, L. (2008). Experimental study of beam-column behavior of steel single angles: *Journal of Constructional Steel Research*, **Vol.64**, 505-514

Takahashi, O., Hirano, M., Hozumi, H. and Kaneko, S. (1991). Experimental studies on the collapse behavior of bracing under cyclic loadings : Part1 : Angle steel. *The AIJ annual meeting (1991)*. C, 1431-1432 (in Japanese).

The Buliding Standard Law of Japan (2007), The building center of Japan

The Architectural Institute of Japan (2005). Design Standard for Steel Structures –Allowable Stress Design-. The Architectural Institute of Japan

Yoo, J., Rooder, C. and Lehman, D. (2009) Simulated behavior of multi-story X-braced frames, *Engineering Structures*, **vol.31**, 182-197

The Japanese Industry Standard (2004). JIS B 3101. Rolled Steels for General Structures.